nature physics

SUPPLEMENTARY INFORMATION

DOI: 10.1038/NPHYS3356

# Unidirectional spin Hall magnetoresistance in ferromagnet/normal metal bilayers

Can Onur Avci, Kevin Garello, Abhijit Ghosh, Mihai Gabureac, Santos F. Alvarado, and Pietro Gambardella

*Department of Materials, ETH Zürich, Hönggerbergring 64, CH-8093 Zürich, Switzerland*

## CONTENTS

DOI: 10.1038/NPHYS3356

## SI 1. HARMONIC ANALYSIS OF THE LONGITUDINAL AND HALL RESISTANCES

The longitudinal resistance ($R$) and transverse (Hall) resistance ($R^H$) are measured by applying an ac current $I = I_0 \sin(\omega t)$ of constant amplitude $I_0$ and frequency $\omega/2\pi = 10$ Hz and recording the ac longitudinal ($V$) and transverse ($V^H$) voltage, respectively. Ohm's law for a current-dependent resistance reads $V(I) = R(I) \cdot I_0 \sin(\omega t)$. Assuming that the current-induced resistance changes are small with respect to the linear resistance of the sample, $R(0)$, we can expand $R$ and $V$ as follows:

$$R(I) = R(0) + \frac{dR}{dI} dI = R(0) + \frac{1}{2} I_0 \frac{dR}{dI} \sin(2\omega t)\,, \tag{S1}$$

and

$$V(I) = I_0 R(0) \sin(\omega t) + \frac{1}{2} I_0^2 \frac{dR}{dI} \sin(2\omega t)\,, \tag{S2}$$

where the longitudinal voltage consists of first and second harmonic terms that scale with $I_0$ and $I_0^2$, respectively. Accordingly, we define the first and second harmonic resistance as $R_\omega = R(0)$ and $R_{2\omega} = \frac{1}{2} I_0 \frac{dR}{dI}$. Analogue expansions apply to the first and second harmonic Hall resistances, $R^H_\omega$ and $R^H_{2\omega}$. The first harmonic terms can be written as

$$R_\omega = R^z + (R^x - R^z) \sin^2\theta \cos^2\varphi + (R^y - R^z) \sin^2\theta \sin^2\varphi\,, \tag{S3}$$

$$R^H_\omega = R_{AHE} \cos\theta + R_{PHE} \sin^2\theta \sin(2\varphi)\,, \tag{S4}$$

where $\theta$ and $\varphi$ are the polar and azimuthal magnetization angles, $R^i$ is the longitudinal resistance measured when the magnetization is saturated parallel to the direction $i = x, y, z$, and $R_{AHE}$ and $R_{PHE}$ are the anomalous Hall and planar Hall coefficients, respectively. Note that Eqs. S3 and S4 simply represent the conventional magnetoresistance (MR) and Hall resistance. The second harmonic terms, on the other hand, include all the contributions to $V$ and $V^H$ that vary quadratically with the current, specifically: the MR and Hall resistance changes due to current-induced spin-orbit torques (SOT) and Oersted field[S1–S4], thermoelectric effects[S5,S6], and nonlinear resistive terms. We have previously studied the influence of the SOT and thermal gradients ($\nabla T$) on the transverse voltage, showing that the corresponding second harmonic Hall resistances, $R^{H,SOT}_{2\omega}$ and $R^{H,\nabla T}_{2\omega}$, can be separately measured due to their different symmetry and field dependence[S6]. In this paper we show there is an additional nonlinear contribution that adds to the longitudinal resistance, which we call unidirectional spin Hall magnetoresistance (USMR). We thus have

$$R_{2\omega} \propto I_0 (R^{SOT}_{2\omega} + R^{\nabla T}_{2\omega} + R^{USMR}_{2\omega})\,, \tag{S5}$$

$$R^H_{2\omega} \propto I_0 (R^{H,SOT}_{2\omega} + R^{H,\nabla T}_{2\omega})\,. \tag{S6}$$

The SOT terms are due to the current-induced oscillations of the magnetization that modulate the MR and Hall resistance through the dependence of the angles $\theta$ and $\varphi$ on the current. These terms read, for the longitudinal and transverse case, as

$$R^{SOT}_{2\omega} = I_0[(R^x - R^z)\cos^2\varphi + (R^y - R^z)\sin^2\varphi] \frac{d\sin^2\theta}{dI} + I_0[(R^y - R^z)\sin^2\theta - (R^x - R^z)\sin^2\theta] \frac{d\sin^2\varphi}{dI}\,, \tag{S7}$$

$$R^{H,SOT}_{2\omega} = I_0 (R_{AHE} - 2R_{PHE}\cos\theta \sin 2\varphi) \frac{d\cos\theta}{dI} + I_0 R_{PHE} \sin^2\theta \frac{d\sin 2\varphi}{dI}\,. \tag{S8}$$

The thermoelectric terms are due to Joule heating and corresponding quadratic increase of the sample temperature with current, which gives rise to temperature gradients[S6]:

$$\nabla T \propto I_0^2 \sin^2(\omega t) R_0 = \frac{1}{2} I_0^2 [1 - \cos(2\omega t)] R_0\,. \tag{S9}$$

Such thermal gradients can give rise to the anomalous Nernst[S7,S8], spin Seebeck[S9] and magneto-thermopower effects[S7] with distinct angular dependencies. Their functional form in the longitudinal and transverse geometries is given in Sect. SI 4 for an arbitrary $\nabla T$.

Finally, the modulation of the ferromagnet/normal metal (FM/NM) interface resistance by the spin Hall effect (SHE) gives rise to a second harmonic term

$$R_{2\omega}^{USMR} \propto I_0 \theta_{SH} M_y \,, \tag{S10}$$

where $\theta_{SH}$ is the spin Hall angle of the NM and $M_y$ the $y$ component of the magnetization of the FM (see Figure 1 of the main text for the definition of the spatial coordinates).

## SI 2. DETERMINATION OF THE POLAR MAGNETIZATION ANGLE USING THE HALL RESISTANCE

If the magnetization is fully aligned to the external field, the polar and azimuthal angles of the **M** and **B** vectors coincide ($\theta = \theta_B$ and $\varphi = \varphi_B$). Even for magnetic fields of the order of a few Tesla, however, the demagnetizing field induces a significant deviation of $\theta$ from $\theta_B$, while, in the case of easy plane anisotropy of interest here, $\varphi = \varphi_B$ remains true. In order to fit the angular dependence of the MR in the $zx$, $zy$, and $xy$ planes using Eq. S3, we therefore need an independent measurement of $\theta$. This is easily performed by measuring the Hall resistance as a function of $\theta_B$ in the $zx$ ($\varphi = 0$) or $zy$ ($\varphi = \pi/2$) planes, as $R_\omega^H$ simplifies to $R_\omega^H = R_{AHE} \cos\theta$ in this case. The saturation value of the anomalous Hall resistance, $R_{AHE}$, is obtained as shown in Fig. S1, where we report the Hall resistance for the $zy$ angular scans corresponding to (a) Ta(6nm)|Co(2.5nm) and (b) Pt(6nm)|Co(2.5nm), simultaneously recorded during the magnetoresistance (MR) measurements shown in Fig. 2 of the main text. A nearly identical $R_\omega^H$ is detected in the $zx$ plane for both samples. The insets show $R_\omega^H$ measured as a function of external field parallel to $z$, showing that the magnetization is technically saturated at a field of $\pm 1.7$ T. Note that the saturation field of Ta|Co ($\sim 1.45$ T) is larger than that of Pt|Co ($\sim 0.8$ T) because of the strong perpendicular magnetic anisotropy (PMA) of Pt|Co, which counters the demagnetizing field of the Co layer.

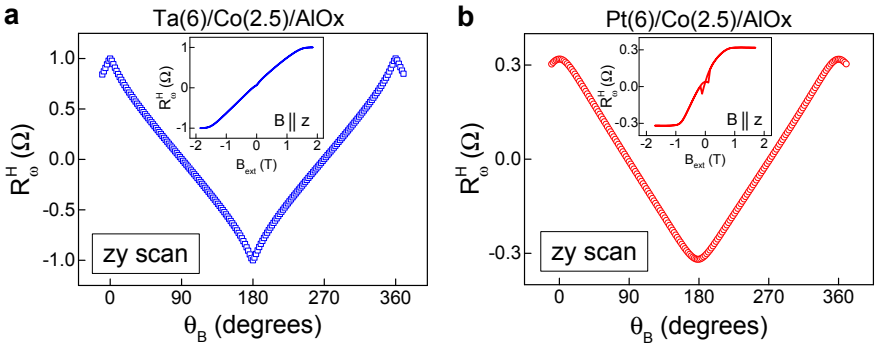


FIG. S1. **Anomalous Hall resistance measurements.** **a,** $R_\omega^H = R_{AHE}\cos\theta$ of Ta(6nm)|Co(2.5nm) and **b,** Pt(6nm)|Co(2.5nm) measured during a $zy$ scan at fixed external field $B = 1.7$ T. A small constant offset due to misalignment of the Hall branches has been subtracted from both curves. Insets: $R_\omega^H$ as a function of out-of-plane field. The features around $B_{ext} = 0$ T are due to planar Hall effect contributions.

## SI 3. INFLUENCE OF SPIN-ORBIT TORQUES ON THE SECOND HARMONIC MR MEASUREMENTS

An electric current flowing in the plane of a FM/NM bilayer generates two qualitatively different types of SOT: a field-like (FL) torque $\boldsymbol{\tau}_{FL} \sim \mathbf{M} \times \hat{\mathbf{y}}$, and an antidamping-like (AD) torque $\boldsymbol{\tau}_{AD} \sim \mathbf{M} \times (\hat{\mathbf{y}} \times \mathbf{M})$, where $\hat{\mathbf{y}}$ is the in-plane axis perpendicular to the current flow direction $\hat{\mathbf{x}}$ (Refs. S1, S4, S10–S12). The action of these torques is

DOI: 10.1038/NPHYS3356

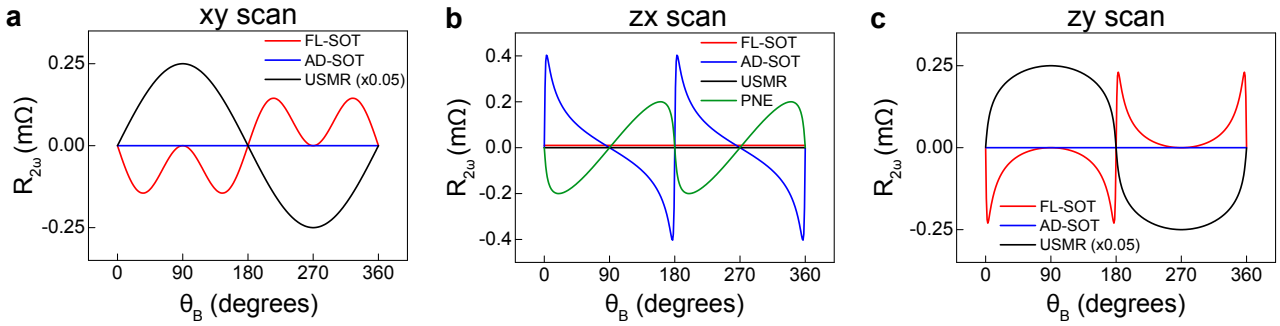


FIG. S2. **Macrospin simulations of $R_{2\omega}^{SOT}$ and $R_{2\omega}^{USMR}$. a,** $xy$ scan, **b,** $zx$ scan, and **c,** $zy$ scan simulations. The simulated planar Nernst signal is also shown for comparison in **b**. Note that the SOT signals are approximately a factor 20 smaller compared to the USMR in the $xy$ and $zy$ plane. This is due to the fact that the magnetization becomes less susceptible to the current-induced torques when $\boldsymbol{\tau}_B$ is much larger compared to $\boldsymbol{\tau}_{AD}$ and $\boldsymbol{\tau}_{FL}$.

equivalent to that of two effective fields $\mathbf{B}_{FL} \sim \mathbf{M} \times \boldsymbol{\tau}_{FL}$ and $\mathbf{B}_{AD} \sim \mathbf{M} \times \boldsymbol{\tau}_{AD}$ perpendicular to the instantaneous direction of the magnetization .

Most of the studies using harmonic measurements so far have employed the Hall effect to reveal and quantify the SOT[S1–S4,S13]. However, SOT also give rise to second harmonic MR signals, $R_{2\omega}^{SOT}$, as noted in Ref. S3. Here we analyze the angular dependence of $R_{2\omega}^{SOT}$ based on symmetry arguments and macrospin simulations of the MR. To perform the simulations we compute the equilibrium position of $\mathbf{M}$ by considering the sum of all the torques acting on it: the torque due to the external field ($\boldsymbol{\tau}_B$), PMA ($\boldsymbol{\tau}_{PMA}$), demagnetizing field ($\boldsymbol{\tau}_{DEM}$), as well as the field-like SOT, including the torque due to the Oersted field, ($\boldsymbol{\tau}_{FL}$), and the antidamping-like SOT ($\boldsymbol{\tau}_{AD}$). At equilibrium, the position of the magnetization is defined by:

$$\boldsymbol{\tau}_B + \boldsymbol{\tau}_{PMA} + \boldsymbol{\tau}_{DEM} + \boldsymbol{\tau}_{FL} + \boldsymbol{\tau}_{AD} = 0 \tag{S11}$$

We numerically solve the above equation for the equilibrium angles of the magnetization $\theta$ and $\varphi$ as a function of external field and current, using measured values of the following parameters for Ta(6nm)|Co(2.5nm): $R^x - R^y = 1.36\ \Omega$, $R^z - R^y = 0.82\ \Omega$, $R^H = 1\ \Omega$, $R^{PNE} = 0.2$ m$\Omega$, $\boldsymbol{\tau}_{FL} = 0.24$ mT, $\boldsymbol{\tau}_{AD} = 0.6$ mT, $\boldsymbol{\tau}_{DEM} = 1.45$ T, and $\boldsymbol{\tau}_{PMA} \approx 0$. Figures S2a-c compare the simulations of the second harmonic MR due to the SOT (Eq. S7) and USMR (Eq. S10) in the $xy$, $zx$, and $zy$ planes for an external field $B_{ext} = 1.7$ T and current density $j = 10^7$ A/cm$^2$. The simulations show that the FL torque can give rise to a second harmonic MR contribution in the $xy$ and $zy$ scans whereas the contribution due to the AD torque is equally zero in both cases. In the $zx$ scan we have the opposite behavior, i.e., that the FL torque gives no contribution, whereas the AD torque gives rise to a non-zero signal. However, in all cases the MR contributions with SOT origin have a distinct symmetry with respect to the measurements reported in Fig. 2 of the main text. Moreover, $R_{2\omega}^{SOT} = 0$ when either $\varphi_B$ or $\theta_B = \pi/2$ excluding the influence of SOT on the USMR measurements.

## SI 4. THERMOELECTRIC EFFECTS

Thermoelectric effects must be carefully considered in the measurement of electrical signals due to unavoidable Joule heating and consequent temperature gradients in the sample. The thermal gradient can have an arbitrary direction depending on the device geometry, stacking order of the layers, inhomogeneous current flow due to resistivity inhomogeneities in each device and give rise to a second harmonic signal, $R_{2\omega}^{\nabla T}$, due to their quadratic dependence on the injected current. A proper analysis incorporates the Nernst and Seebeck effects considering temperature gradients in all three directions in space. We have treated these effects case-by-case to identify their symmetry and their possible contribution to $R_{2\omega}^{\nabla T}$.

The anomalous Nernst effect (ANE) is analogous to the anomalous Hall effect driven by a temperature gradient[S5,S7]. The symmetry of the electric field driven by the ANE that gives rise to a second harmonic signal is as following:

$$\mathbf{E}_{ANE} = -\alpha \nabla \mathbf{T} \times \mathbf{M}\,, \tag{S12}$$

where $\alpha$ is the material dependent ANE coefficient. By considering an arbitrary temperature gradient $\nabla\mathbf{T} = (\nabla T_x, \nabla T_y, \nabla T_z)$ and magnetization direction $\hat{\mathbf{M}} = (\sin\theta\cos\varphi, \sin\theta\sin\varphi, \sin\theta)$ we find the following allowed symmetries for the second harmonic longitudinal ($R_{2\omega}^{\nabla T}$) and transverse ($R_{2\omega}^{H,\nabla T}$) resistances:

$$R_{2\omega}^{ANE} \propto \nabla T_y \cos\theta - \nabla T_z \sin\theta \sin\varphi\,, \tag{S13}$$

$$R_{2\omega}^{H,ANE} \propto \nabla T_z \sin\theta \cos\varphi - \nabla T_x \cos\theta\,. \tag{S14}$$

The anisotropic magneto-thermopower (AMTEP) is the magnetization-dependent Seebeck effect and is the thermal analogous of the magnetoresistance[S14]. Therefore, its manifestation follows Eq. S3 and, in terms of temperature gradients, reads:

$$R_{2\omega}^{AMTEP} \propto \nabla T_x(\sin^2\theta\cos^2\varphi + \sin^2\theta\sin^2\varphi)\,, \tag{S15}$$

$$R_{2\omega}^{H,AMTEP} \propto \nabla T_y(\sin^2\theta\cos^2\varphi + \sin^2\theta\sin^2\varphi)\,. \tag{S16}$$

The transverse manifestation of the AMTEP, the so-called planar Nernst effect (PNE)[S15,S16], is analogous to the planar Hall effect and reads:

$$R_{2\omega}^{PNE} \propto \nabla T_y \sin^2\theta \sin 2\varphi + \nabla T_z \sin 2\theta \cos^2\varphi\,, \tag{S17}$$

$$R_{2\omega}^{H,PNE} \propto \nabla T_x \sin^2\theta \sin 2\varphi + \nabla T_z \sin 2\theta \sin^2\varphi\,. \tag{S18}$$

In addition to these signals, in FM/NM bilayers one has to take into account the spin Seebeck effect (SSE), whereby a thermal gradient can drive a spin current that can be detected as a voltage across the bilayer via the inverse spin Hall effect. In our measurement geometry we could, in principle, observe the longitudinal SSE[S9] due to a perpendicular thermal gradient, which would give rise to a signal with identical symmetry as that of the ANE (Eq. S13 and Eq. S14)[S8], although its sign would depend on the sign of the spin Hall effect in the NM layer.

By considering Eq. S13 through Eq. S18 we notice that only a signal originating from the ANE (possibly including also the longitudinal SSE) and due to $\nabla T_z$ possesses the same symmetry as that of the USMR ($R_{2\omega}^{USMR} \propto \sin\theta\sin\varphi$). In the following, we discuss how these two effects can be separated. In previous work, we have shown that the ANE driven by a perpendicular temperature gradient induces a nonzero second harmonic Hall resistance in Co layers[S6]. We use an 8 nm thick Co sample as a reference to reveal the influence of the ANE on the second harmonic longitudinal resistance. Figure S3 shows the first and second harmonic signals of longitudinal and transverse measurements when $\mathbf{M}$ is rotated in the $xy$ plane in a fixed field $B = 0.4$ T. Sinusoidal fits (red solid curves) confirm the expected MR (planar Hall effect) symmetry in the longitudinal (transverse) first harmonic signals and the ANE symmetry in the second harmonic signals. Since the MR and planar Hall effect have the same microscopic origin, their amplitude is proportional to the physical distance over which they are measured. The same holds for the longitudinal and transverse ANE signals, which implies that the ratio between the longitudinal and transverse MR and ANE measurements is equal to the length/width ($l/w$) ratio of the Hall bar. This was verified experimentally by measuring the ratio $l/w$ of our Hall bars using scanning electron microscopy for devices of different size and including other reference layers such as Ti|Co bilayers for which the ANE and MR coefficients differ from those of a single Co layer[S6]. Therefore, by

DOI: 10.1038/NPHYS3356

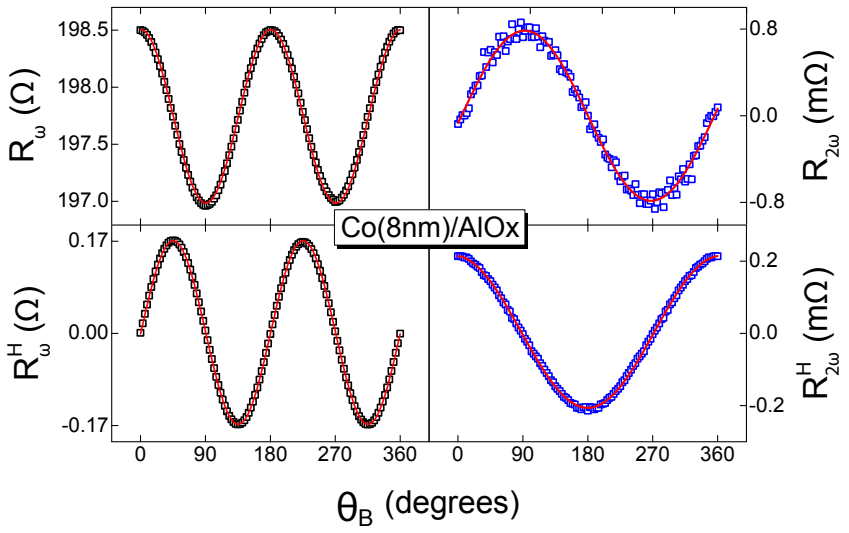


FIG. S3. **Longitudinal and transverse measurements of the MR and ANE in a single Co layer.** First and second harmonic signals corresponding to the longitudinal and transverse resistance of Co(8nm). The sinusoidal fits (red curves) to the first harmonic signals show that the magnetization follows the applied field direction and the angular dependence of the MR ($R_\omega$) and planar Hall effect ($R^H_\omega$), whereas the second harmonic signals have the angular dependence expected of the ANE according to Eqs. S13 and S14. Note that $R_{2\omega}/R^H_{2\omega} = 4 = l/w$ as measured by scanning electron microscopy for this device.

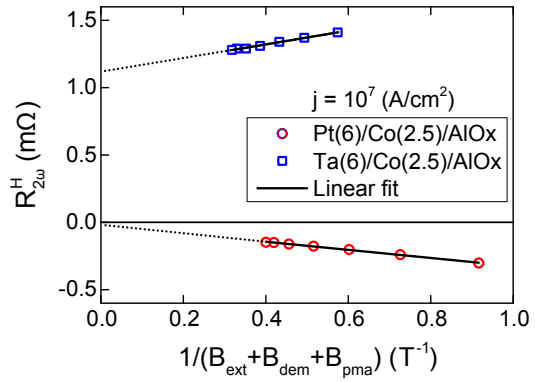


FIG. S4. **Separation of AD-SOT and ANE contributions to $R^H_{2\omega}$.** Plot of the cosine component of $R^H_{2\omega}$ due to the AD-SOT and ANE as a function of $(B_{ext} + B_{DEM} + B_{PMA})^{-1}$ measured in an $xy$ scan for Ta(6nm)|Co(2.5nm) and Pt(6nm)|Co(2.5nm).

measuring the thermal signal in the transverse geometry one can accurately determine its sign and magnitude in the longitudinal measurements.

In FM/NM bilayers we must additionally consider the fact that the transverse thermoelectric signal, $R^{H,\nabla T}_{2\omega}$, is mixed with $R^{H,SOT}_{2\omega}$. These two effects, however, can be separated in a quantitative way as shown in Ref. S6 and explained briefly below. During an $xy$ scan of the magnetization, the FL-SOT gives a contribution to $R^H_{2\omega}$ proportional to $\cos 3\varphi + \cos\varphi$, whereas the AD-SOT and the ANE both give a contribution proportional to $\cos\varphi$. The AD-SOT and ANE contributions can be further separated by considering that the AD-SOT induces dynamical oscillations of the magnetization, the amplitude of which is proportional to the magnetic susceptibility of the FM layer. The resulting $R^{H,SOT}_{2\omega}$ signal therefore depends on the susceptibility of the magnetization, which decreases with increasing external field, whereas the ANE contribution is constant provided that the magnetization is saturated along the field

direction, as is the case in our measurements. The $\cos\varphi$ component of $R^{H}_{2\omega}$ is in fact a linear function of the inverse of the effective magnetic fields acting on the magnetization, $(B_{ext} + B_{DEM} + B_{PMA})^{-1}$, with slope proportional to the AD-SOT and intercept proportional to the ANE[S6]. Figure S4 shows a plot of this component for two of the samples used in this study, Ta(6nm)|Co(2.5nm) and Pt(6nm)|Co(2.5nm). The intercept of the linear fit gives a non-negligible ANE-induced signal in the case of Ta ($R^{H,\nabla T}_{2\omega} = 1.1$ m$\Omega$), whereas a negligible ANE is found for the Pt sample ($R^{H,\nabla T}_{2\omega} = 0.02$ m$\Omega$). The corresponding MR of thermal origin is then given by $R^{\nabla T}_{2\omega} = \frac{l}{w} R^{H,\nabla T}_{2\omega}$. The above study is repeated for all the samples used in this work to separate the thermoelectric contributions from the measured second harmonic MR and reveal the pure USMR signal, given by $R^{USMR}_{2\omega} = R_{2\omega} - R^{\nabla T}_{2\omega}$.

## SI 5. ABSENCE OF THE USMR IN SINGLE LAYER SAMPLES

The measurements presented in Fig. S3 exclude the existence of a net USMR signal for a single Co layer. In order to further verify if the USMR is due to the Co/NM interface or to another nonlinear mechanism giving rise, e.g., to a self-induced MR induced by the SHE, such as that due to edge spin accumulation predicted by Dyakonov[S17], we have grown two Ta(6nm) and Pt(6nm) reference layers and measured $R_\omega$ and $R_{2\omega}$ for these samples. Figure S5 shows the $zy$ scans for Ta (upper panels) and Pt (lower panels). The measurements are performed using a current density $j = 0.2 \cdot 10^7$ A/cm$^2$ for Ta and $j = 10^7$ A/cm$^2$ for Pt. The lower current density used for the Ta layer is due to the input voltage limit of our acquisition system and the high resistivity of Ta. Within the sensitivity of our measurements, we do not observe any systematic magnetic field dependence of either $R_\omega$ or $R_{2\omega}$, which excludes any influence from the NM layer alone in the USMR.

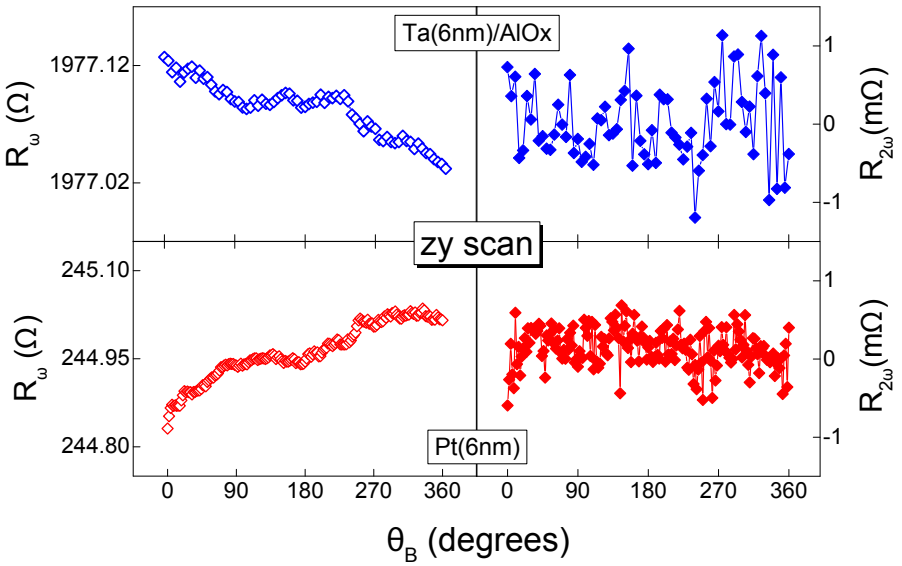


FIG. S5. **Measurements of $R_\omega$ or $R_{2\omega}$ in single Ta and Pt layers.** First (left) and second (right) harmonic longitudinal resistance signals in Ta(6nm) (top) and Pt(6nm) (bottom) reference layers. Due to the high resistivity of Ta, the Ta data are averaged over five $zy$ scans performed with $B_{ext} = 1.7$ T and $j = 0.2 \cdot 10^7$ A/cm$^2$. For Pt, a single $zy$ scan is shown with $j = 10^7$ A/cm$^2$ and $B_{ext} = 1.9$ T.

DOI: 10.1038/NPHYS3356

## SI 6. USMR IN Ta|Cu|Co LAYERS

In order to elucidate the possible role of the FM-induced magnetization in the NM, we have inserted a Cu spacer with thickness 2 and 4 nm between Ta and Co. The choice of Cu is motivated by its large spin diffusion length as well as by its low and short-range induced magnetization. Ta(6nm)|Co(2.5nm) was chosen as a test system because of the larger absolute amplitude of the USMR relative to Pt. The aim of this study is twofold. First, to see if the USMR is still present when the Ta and Co layers are physically separated. Second, to examine if there is any influence of the induced magnetization on the reported USMR signal, although, judging by the change of sign of the USMR observed in the Ta|Co and Pt|Co layers, this appears unlikely. If the induced magnetization plays a role, we do not expect to measure a USMR signal after the insertion of the Cu spacer layers. However, if the USMR is due to the current-induced spin accumulation at the FM/NM interface, we expect to measure $R_{2\omega}^{USMR} \neq 0$ but reduced in amplitude with respect to Ta|Co, mainly due to current shunting in the Cu layer.

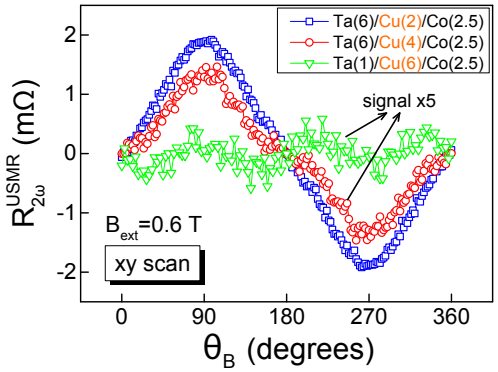


FIG. S6. **Influence of a Cu spacer layer on the USMR signal of Ta|Co.** $xy$ scan of $R_{2\omega}^{USMR}$ measured in Ta(1,6nm)|Cu(2-6nm)|Co(2.5nm) trilayers with current density $j = 10^7$ A/cm$^2$.

Figure S6 shows the USMR of Ta(1,6nm)|Cu(2-6nm)|Co(2.5nm) layers. We observe a clear signal in Ta(6nm)|Cu(2,4nm)|Co(2.5nm) that has the same sign as that measured in Ta(6nm)|Co(2.5nm). As expected, the USMR decreases significantly with increasing Cu layer thickness, from 1.9 mΩ for Ta(6nm)|Cu(2nm)|Co(2.5nm) to 0.28 mΩ for Ta(6nm)|Cu(4nm)|Co(2.5nm), and so does the resistivity of the devices, from 54.6 $\mu\Omega$cm to 34.1 $\mu\Omega$cm, showing that the shunting effect of Cu quickly dominates the conduction. The sample with Ta(1nm) has a resistivity of 16.9 $\mu\Omega$cm and serves as a reference to show that the USMR vanishes if the conduction is dominated by the Co/Cu bilayer, due to the negligible SHE of Cu. We note that the 1 nm of Ta was deposited as an adhesion layer for Cu on the SiO substrate and that its conductivity is expected to be negligibly small due to oxidation and the much larger resistivity of Ta relative to Cu. Overall, these data confirm that the USMR is dominated by the spin accumulation at the FM/NM interface induced by the SHE in the heavy metal layer and that the induced magnetization in the NM does not play a significant role.

## SI 7. SPIN ACCUMULATION AND POTENTIAL SHIFT INDUCED BY THE SHE IN A FM/NM BILAYER

There are essentially two effects that are important to interpret the USMR and model its dependence on the thickness of the NM layer. One is the buildup of the SHE-induced spin accumulation at the FM/NM interface, which occurs over a length-scale comparable to the spin diffusion length of the NM, and the other is a dilution effect due to reduced number of electrons that scatter at the interface relative to the total number of electrons participating to the conduction. We consider these two effects separately.

Our first point is the assumption that the USMR is proportional to the nonequilibrium spin accumulation at the FM/NM interface induced by the in-plane charge current. As explained in the text, this is motivated by the

modulation of the conductivity mismatch that exists at the interface between a FM and a NM due to the SHE-induced change of majority and minority spin populations. In order to calculate the spin accumulation, we adopt the drift-diffusion approach[S18,S19]. The spin accumulation is defined as $\boldsymbol{\mu}_s = \boldsymbol{\mu}^{\uparrow} - \boldsymbol{\mu}^{\downarrow}$, where $\boldsymbol{\mu}^{\uparrow}$ and $\boldsymbol{\mu}^{\downarrow}$ represent the spin-dependent electrochemical potentials for majority ($\uparrow$) and minority ($\downarrow$) electrons. We recall that the nonequilibrium magnetization in the NM is $\delta\mathbf{m} = -\mathcal{N}(\varepsilon_F)\mu_B\boldsymbol{\mu}_s$, where $\mathcal{N}(\varepsilon_F)$ is the density of states at the Fermi level and the minus sign stems from the opposite orientation of the magnetic spin moment and spin angular moment.

We consider a bilayer consisting of a NM with electrical conductivity $\sigma_N$, spin diffusion length $\lambda_N$, and thickness $t_N$, and a FM defined by the analogous quantities $\sigma_F$, $\lambda_F$, and $t_F$. The conductivity of the FM is assumed to be the sum of the independent conductivities for the majority and minority electrons: $\sigma_F = \sigma^{\uparrow} + \sigma^{\downarrow}$. Accordingly, the current flowing in the FM has a net spin polarization $P = (\sigma^{\uparrow} - \sigma^{\downarrow})/(\sigma^{\uparrow} + \sigma^{\downarrow})$. We define $x$ as the current direction and $z$ as the direction normal to the interface; the interface plane is situated at $z = 0$. The source term for $\boldsymbol{\mu}_s$ is the spin current generated inside the NM by the SHE and propagating along $z$:

$$\mathbf{j}_s^0 = j_{SH}^0(\hat{\mathbf{j}} \times \hat{\mathbf{z}}) = -j_{SH}^0\hat{\mathbf{y}} = -\theta_{SH}\sigma_N E_x\hat{\mathbf{y}}\,, \tag{S19}$$

where $\hat{\mathbf{y}}$ represents the spin polarization direction, $E_x$ the electric field driving the charge current $\mathbf{j}$ through the bilayer, and $\theta_{SH}$ the spin Hall angle of the NM. The spin Hall angle of the FM is assumed to be zero. This approximation neglects the spin and charge accumulation induced by the anomalous Hall effect at the boundaries of the FM, which can be included in more detailed calculations but are not essential to the arguments developed here. Furthermore, we assume that the magnetization of the FM is saturated parallel to $\pm\hat{\mathbf{y}}$. In this case, there are no sink terms for the spin current inside the FM other than spin-flip relaxation; in particular, the spin current associated to the SOT via the real and imaginary part of the spin-mixing conductance ($G_{\uparrow\downarrow}$) vanishes[S20]:

$$\mathbf{j}_s^{SOT} \sim \mathrm{Re}\{G_{\uparrow\downarrow}\}\boldsymbol{\tau}_{AD} + \mathrm{Im}\{G_{\uparrow\downarrow}\}\boldsymbol{\tau}_{FL} \sim \mathrm{Re}\{G_{\uparrow\downarrow}\}\mathbf{M} \times (\hat{\mathbf{y}} \times \mathbf{M}) + \mathrm{Im}\{G_{\uparrow\downarrow}\}(\mathbf{M} \times \hat{\mathbf{y}}) = 0\,. \tag{S20}$$

With this assumption the spin diffusion equation governing the spin accumulation reduces to a one-dimensional problem:

$$\nabla^2\mu_{s_{F,N}}(z) = \frac{\mu_{s_{F,N}}(z)}{\lambda_{F,N}^2}\,, \tag{S21}$$

where $\mu_{s_{F,N}}$ is the $y$ component of the spin accumulation vector in either the FM or the NM layer. The spin current $\mathbf{j}_s = j_s\hat{\mathbf{y}}$ is then given by

$$j_{s_N}(z) = -\frac{\sigma_N}{2e}\partial_z(\mu_N^{\uparrow} - \mu_N^{\downarrow}) - j_{SH}^0 \qquad \text{in the NM layer} \quad (z < 0)\,, \tag{S22}$$

$$j_{s_F}(z) = -\frac{1}{e}\partial_z(\sigma^{\uparrow}\mu_F^{\uparrow} - \sigma^{\downarrow}\mu_F^{\downarrow}) \qquad \text{in the FM layer} \quad (z > 0)\,. \tag{S23}$$

The general solutions of Eq. S21 read

$$\left.\begin{aligned}\mu_N^{\uparrow}(z) &= A_N + B_N z + C_N\exp(z/\lambda_N) + D_N\exp(-z/\lambda_N)\\ \mu_N^{\downarrow}(z) &= A'_N + B'_N z + C'_N\exp(z/\lambda_N) + D'_N\exp(-z/\lambda_N)\end{aligned}\right\} z < 0 \tag{S24}$$

$$\left.\begin{aligned}\mu_F^{\uparrow}(z) &= A_F + B_F z + C_F\exp(z/\lambda_F) + D_F\exp(-z/\lambda_F)\\ \mu_F^{\downarrow}(z) &= A'_F + B'_F z + C'_F\exp(z/\lambda_F) + D'_F\exp(-z/\lambda_F)\end{aligned}\right\} z > 0 \tag{S25}$$

The coefficients appearing in Eqs. S24, S25 are determined by imposing charge conservation $\nabla\cdot\mathbf{j} = 0$ in the two layers:

$$\partial_z^2\left(\frac{\sigma_N}{2}\mu_N^{\uparrow} + \frac{\sigma_N}{2}\mu_N^{\downarrow}\right) = 0 \qquad z < 0\,, \tag{S26}$$

$$\partial_z^2(\sigma^{\uparrow}\mu_F^{\uparrow} + \sigma^{\downarrow}\mu_F^{\downarrow}) = 0 \qquad z > 0\,, \tag{S27}$$

and by the following boundary conditions:

1. The net charge flow perpendicular to the FM/NM interface is zero:

$$j_F^{\uparrow} + j_F^{\downarrow} = j_N^{\uparrow} + j_N^{\downarrow} = 0. \tag{S28}$$

DOI: 10.1038/NPHYS3356

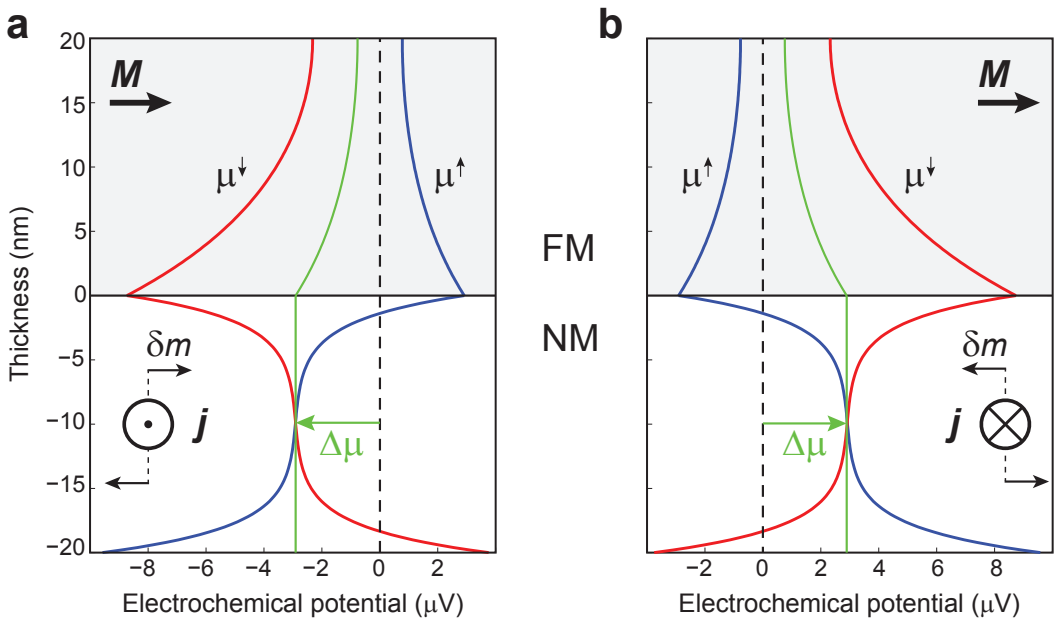


FIG. S7. **Spin accumulation and modulation of the spin-dependent electrochemical potential by the SHE.** Profile of the electrochemical potential of majority ($\mu^{\uparrow}$, blue lines) and minority ($\mu^{\downarrow}$, red lines) electrons in proximity of the FM/NM interface calculated using Eqs. S24-S25 for **a,** positive and **b,** negative current. The electrochemical potential of the NM shifts relative to that of the FM as indicated by the green arrow. The direction of the magnetization is $\mathbf{M} \parallel \hat{\mathbf{y}}$ in both panels.

2. The spin-dependent current components are continuous across the FM/NM interface:

$$j_F^{\uparrow,\downarrow}(0) = j_N^{\uparrow,\downarrow}(0). \tag{S29}$$

3. The discontinuity of the electrochemical potentials of majority and minority electrons at the FM/NM interface is proportional to the spin-dependent boundary resistances $r^{\uparrow}$ and $r^{\downarrow}$, respectively:

$$\mu_F^{\uparrow}(0) - \mu_N^{\uparrow}(0) = er^{\uparrow}j^{\uparrow}(0) \quad \text{and} \quad \mu_F^{\downarrow}(0) - \mu_N^{\downarrow}(0) = er^{\downarrow}j^{\downarrow}(0). \tag{S30}$$

4. The spin current vanishes at the bottom of the NM layer and at the top of the FM layer:

$$j_{s_N}(-t_N) = j_{s_F}(t_F) = 0. \tag{S31}$$

In Eqs. S28-S30 above we have introduced the majority and minority current components, $j_F^{\uparrow,\downarrow} = \frac{\sigma_F^{\uparrow,\downarrow}}{e}\partial_z \mu_F^{\uparrow,\downarrow}$ and $j_N^{\uparrow,\downarrow} = \frac{\sigma_N}{2e}\partial_z \mu_N^{\uparrow,\downarrow} \mp \frac{1}{2} j_{SH}^0$, where the "majority" direction in the NM is defined with respect to that of the FM. The boundary condition S29 implies the continuity of the spin current, $j_{s_F}(0) = j_{s_N}(0)$, which is justified only in the absence of spin-flip scattering at the interface[S19]. To simplify our model, we assume this to be the case even if spin-flip scattering at the Co|Pt interface can reduce the spin current by as much as a factor two[S21]. In Eq. S30 we retain the effects of interface scattering due to the different band structure of the NM and FM and diffuse scattering by the roughness or chemical disorder of the interface, which are relevant in the theory of CIP-GMR[S22]. The spin-dependent boundary resistances are defined in analogy with the spin-dependent resistivity in bulk FM:

$$r_{\uparrow(\downarrow)} = 2r_b(1 - (+)\gamma), \tag{S32}$$

where $r_b = (r_\uparrow + r_\downarrow)/4$ is the interface resistance (in units of $\Omega m^2$) and $\gamma = (r_\downarrow - r_\uparrow)/(r_\uparrow + r_\downarrow)$ the interfacial spin asymmetry coefficient[S19].

Finally, we obtain

$$\mu_{s_N}(0) = \mu_{s_N}^0 \tanh\frac{t_N}{2\lambda_N} \frac{1 + \frac{r_b}{\rho_F\lambda_F}(1-P^2)\tanh\frac{t_F}{\lambda_F}}{1 + \left(\frac{\rho_N\lambda_N}{\rho_F\lambda_F}\coth\frac{t_n}{\lambda_N} - \frac{r_b}{\rho_F\lambda_F}\right)(1-P^2)\tanh\frac{t_F}{\lambda_F}}, \tag{S33}$$

where $\mu^0_{s_N} = 2\,e\,\rho_N\lambda_N\,\theta_{SH}\,j$ is the bare spin accumulation due to the SHE that would be obtained for a single, infinitely thick NM layer and we have substituted the conductivity by the corresponding resistivity parameters $\rho_N = 1/\sigma_N$ and $\rho_F = 1/\sigma_F$. Note that in the limit $\rho_F \to \infty$ we recover the spin accumulation calculated for an insulating FM/NM interface[S20,S23]. Differently from the latter case, however, the SHE induces a shift of the electrochemical potential of the NM layer, $\mu_N = (\mu_N^{\uparrow} + \mu_N^{\downarrow})/2$, relative to that of the FM, $\mu_F = (\mu_F^{\uparrow} + \mu_F^{\downarrow})/2$. Taking $\mu_F(\infty) = 0$ as the reference level, we have

$$\Delta\mu_N = \mu_N - \mu_F(\infty) = -(P + \gamma\tilde{r})\mu^0_{s_N} \tanh\frac{t_N}{2\lambda_N}\frac{1}{1+\tilde{r}}\frac{1}{1+\frac{\frac{\rho_N\lambda_N}{\rho_F\lambda_F}(1-P^2)\tanh\frac{t_F}{\lambda_F}\coth\frac{t_n}{\lambda_N}}{1-\tilde{r}}}, \tag{S34}$$

where $\tilde{r} = \frac{r_b}{\rho_F\lambda_F}(1-P^2)\tanh\frac{t_F}{\lambda_F}$.

By measuring the resistivity of Co, Pt, and Ta reference layers and using published values for $P$, $\lambda_N$, $\lambda_F$, $r_b$, and $\gamma$, it is possible to estimate the relative weight of the different terms appearing in Eqs. S33 and S34. For the resistivity, we obtain $\rho_{Co} = 36.1$ $\mu\Omega$cm, $\rho_{Pt} = 33.4$ $\mu\Omega$cm, and $\rho_{Ta} = 228$ $\mu\Omega$cm. We take $P = 0.31$ and $\lambda_{Co} = 30$ nm from CPP-GMR measurements of Co|Cu films with resistivity similar to ours[S24], $r_b = 0.74$ f$\Omega$m$^2$ and $\gamma = 0.53$ as recently measured for Co|Pt (Ref. S21). Lacking similar measurements for Co|Ta, we assume the same interface resistance values as for Co|Pt. Further, we take $\lambda_{Pt} \approx \lambda_{Ta} \approx 1.5$ nm (Refs. S25 and S26). With these parameters and $t_F = 2.5$ nm, we calculate the products $\frac{\rho_N\lambda_N}{\rho_F\lambda_F}(1-P^2)\tanh\frac{t_F}{\lambda_F} = 0.0034$ (0.023) for Co|Pt (Co|Ta) and $\tilde{r} = 0.005$. Inserting these products into Eqs. S33 and S34, we observe that, for $t_N \gtrsim \lambda_N$, the spin accumulation and the electrochemical potential shift of Co|Pt (Co|Ta) are approximated to within 1% (3%) by

$$\mu_{s_N}(0) \approx \mu^0_{s_N} \tanh\frac{t_N}{2\lambda_N}, \tag{S35}$$

and

$$\Delta\mu_N \approx -P\mu^0_{s_N} \tanh\frac{t_N}{2\lambda_N}. \tag{S36}$$

More generally, we notice that, as long as $t_N \gtrsim \lambda_N$, $t_F < \lambda_F$, $\rho_N\lambda_N < \rho_F\lambda_F$, and $r_b < \rho_F\lambda_F$, both $\mu_{s_N}(0)$ and $\Delta\mu_N$ are mainly determined by the properties of the NM. Figure S7 illustrates the behavior of $\mu^{\uparrow}_{N,F}$, $\mu^{\downarrow}_{N,F}$, and $\Delta\mu_N$ as a function of $z$ calculated using Eqs. S24-S25 and the following parameters: $j = 10^7$ A/cm$^2$, $\theta_{SH} = 0.1$, $P = 0.5$, $\rho_N = \rho_F = 30$ $\mu\Omega$cm, $\lambda_N = 1.5$ nm, $\lambda_F = 10$ nm, $r_b = \gamma = 0$. Figure 5 of the main text reports a similar calculation where $r_b = 0.74$ f$\Omega$m$^2$ and $\gamma = 0.53$ as appropriate for Co|Pt (Ref. S21), which introduces a discontinuity between $\mu_N^{\uparrow,\downarrow}$ and $\mu_F^{\uparrow,\downarrow}$ at $z = 0$.

## SI 8. CURRENT SHUNTING THROUGH THE NM AND FM LAYERS

As the USMR is a pure interface effect, we expect a decrease of $\Delta R^{USMR}$ when the thickness of the NM and FM layers becomes larger than the respective spin diffusion lengths and the current is shunted away from the interface. This effect is similar to the "dilution" of the CIP-GMR observed in FM/NM/FM multilayers[S27]. However, differently from CIP-GMR, the relevant lengthscale beyond which the dilution effect becomes significant here is the spin diffusion length rather than the electron mean free path.

We use a simple parallel resistor model to describe the current flow in a FM/NM bilayer. In this model, the "inactive" regions of the NM and FM layers are described by the resistances $R_N$ and $R_F$ whereas the "active" interface region is described by a linear, current-independent resistance $R_I$ in series with a nonlinear, current-dependent USMR resistance $r_s$. The sign of $r_s$ is determined by the cross product $\mathbf{j}\times\mathbf{M}$. Retaining only first order terms proportional to $r_s$, the equivalent resistance of $R_N$, $R_F$, and $R_I \pm r_s$ connected in parallel is

$$R^{\pm} = \frac{R_I}{1 + R_I\frac{R_N+R_F}{R_N R_F}} \pm r_s\,, \tag{S37}$$

which gives

$$\Delta R^{USMR} = R^+ - R^- = \frac{2r_s}{\left(1 + R_I\frac{R_N+R_F}{R_N R_F}\right)^2}. \tag{S38}$$

DOI: 10.1038/NPHYS3356

To analyze the USMR dependence on the thickness of the NM layer alone, it is practical to include the constant resistance terms $R_F$ and $R_I$ in a single parameter $R_{FI} = R_F R_I/(R_F + R_I)$. We thus obtain

$$\Delta R^{USMR} = \frac{2r_s}{\left(1 + \frac{R_{FI}}{\rho_N}\frac{w}{l}t_N\right)^2}, \tag{S39}$$

and

$$\frac{\Delta R^{USMR}}{R} = \frac{2r_s}{R_{FI}}\frac{1}{1 + \frac{R_{FI}}{\rho_N}\frac{w}{l}t_N}, \tag{S40}$$

where

$$R = \frac{R^+ + R^-}{2} = \frac{R_N R_{FI}}{R_N + R_{FI}} = \frac{R_{FI}}{1 + \frac{R_{FI}}{\rho_N}\frac{w}{l}t_N}, \tag{S41}$$

and $w/l$ is the ratio between the width and the length of the current line.

## SI 9. DEPENDENCE OF THE USMR ON THE THICKNESS OF THE NM LAYER

As argumented in the main text and above, we expect the USMR to be proportional to $\Delta\mu$ times a dilution factor accounting for the shunting of the charge current by the NM layer. Combining Eqs. S35, S39, and S40 we obtain the following phenomenological expressions:

$$\Delta R^{USMR} = A\frac{\tanh\frac{t_N}{2\lambda_N}}{\left(1 + \frac{R_{FI}}{\rho_N}\frac{w}{l}t_N\right)^2}, \quad \frac{\Delta R^{USMR}}{R} = \frac{A}{R_{FI}}\frac{\tanh\frac{t_N}{2\lambda_N}}{1 + \frac{R_{FI}}{\rho_N}\frac{w}{l}t_N}, \tag{S42}$$

where $A$ is a fitting parameter proportional to $P\rho_N\lambda_N\theta_{SH}j$ that accounts also for quantitative differences entering into the calculation of the resistance that escape our model. The values of the free parameters of the fits presented in Fig. 4 of the main text are $A = 7$ mΩ (-14 mΩ) for Ta|Co (Pt|Co), $R_{FI}/\rho_N = 0.08$ nm$^{-1}$ (0.44 nm$^{-1}$), $\lambda_{Ta} = 1.4$ nm and $\lambda_{Pt} = 1.1$ nm.


[1] K. Garello, I. M. Miron, C. O. Avci, F. Freimuth, Y. Mokrousov, S. Blügel, S. Auffret, O. Boulle, G. Gaudin, and P. Gambardella, Nature Nanotech. **8**, 587 (2013).

[2] C. O. Avci, K. Garello, C. Nistor, S. Godey, B. Ballesteros, A. Mugarza, A. Barla, M. Valvidares, E. Pellegrin, A. Ghosh, I. M. Miron, O. Boulle, S. Auffret, G. Gaudin, and P. Gambardella, Phys. Rev. B **89**, 214419 (2014).

[3] M. Hayashi, J. Kim, M. Yamanouchi, and H. Ohno, Phys. Rev. B **89**, 144425 (2014).

[4] J. Kim, J. Sinha, M. Hayashi, M. Yamanouchi, S. Fukami, T. Suzuki, S. Mitani, and H. Ohno, Nature Mater. **12**, 240 (2013).

[5] A. C. Smith, J. F. Janak, and R. B. Adler, *Electronic conduction in solids* (McGraw-Hill New York, 1967).

[6] C. O. Avci, K. Garello, M. Gabureac, A. Ghosh, A. Fuhrer, S. F. Alvarado, and P. Gambardella, Phys. Rev. B **90**, 224427 (2014).

[7] M. Schmid, S. Srichandan, D. Meier, T. Kuschel, J.-M. Schmalhorst, M. Vogel, G. Reiss, C. Strunk, and C. H. Back, Phys. Rev. Lett. **111**, 187201 (2013).

[8] M. Weiler, M. Althammer, F. D. Czeschka, H. Huebl, M. S. Wagner, M. Opel, I.-M. Imort, G. Reiss, A. Thomas, R. Gross, *et al.*, Phys. Rev. Lett. **108**, 106602 (2012).

[9] K. Uchida, H. Adachi, T. Ota, H. Nakayama, S. Maekawa, and E. Saitoh, Appl. Phys. Lett. **97**, 172505 (2010).

[10] K. Ando, S. Takahashi, K. Harii, K. Sasage, J. Ieda, S. Maekawa, and E. Saitoh, Phys. Rev. Lett. **101**, 036601 (2008).

[11] I. M. Miron, G. Gaudin, S. Auffret, B. Rodmacq, A. Schuhl, S. Pizzini, J. Vogel, and P. Gambardella, Nature Mater. **9**, 230 (2010).

[12] P. M. Haney, H.-W. Lee, K.-J. Lee, A. Manchon, and M. Stiles, Phys. Rev. B **87**, 174411 (2013).

[13] U. H. Pi, K. Won Kim, J. Y. Bae, S. C. Lee, Y. J. Cho, K. S. Kim, and S. Seo, Appl. Phys. Lett. **97**, 162507 (2010).
[14] Y. Pu, E. Johnston-Halperin, D. Awschalom, and J. Shi, Phys. Rev. Lett. **97**, 036601 (2006).
[15] V. D. Ky, Phys. Stat. Sol. (b) **22**, 729 (1967).
[16] A. Avery, M. Pufall, and B. Zink, Phys. Rev. Lett. **109**, 196602 (2012).
[17] M. Dyakonov, Phys. Rev. Lett. **99**, 126601 (2007).
[18] P. Van Son, H. Van Kempen, and P. Wyder, Phys. Rev. Lett. **58**, 2271 (1987).
[19] T. Valet and A. Fert, Phys. Rev. B **48**, 7099 (1993).
[20] Y.-T. Chen, S. Takahashi, H. Nakayama, M. Althammer, S. T. Goennenwein, E. Saitoh, and G. E. Bauer, Phys. Rev. B **87**, 144411 (2013).
[21] H. Nguyen, W. Pratt Jr, and J. Bass, J. Magn. Magn. Mat. **361**, 30 (2014).
[22] R. Q. Hood, L. Falicov, and D. Penn, Phys. Rev. B **49**, 368 (1994).
[23] H. Nakayama, M. Althammer, Y.-T. Chen, K. Uchida, Y. Kajiwara, D. Kikuchi, T. Ohtani, S. Geprägs, M. Opel, S. Takahashi, *et al.*, Phys. Rev. Lett. **110**, 206601 (2013).
[24] L. Piraux, S. Dubois, A. Fert, and L. Belliard, Eur. Phys. J. B **4**, 413 (1998).
[25] C. Hahn, G. De Loubens, O. Klein, M. Viret, V. V. Naletov, and J. B. Youssef, Phys. Rev. B **87**, 174417 (2013).
[26] W. Zhang, V. Vlaminck, J. E. Pearson, R. Divan, S. D. Bader, and A. Hoffmann, Appl. Phys. Lett. **103**, 242414 (2013).
[27] B. Dieny, J. Phys. Condens. Matter **4**, 8009 (1992).